SPLIT HOPKINSON PRESSURE BAR IMPULSE EXPERIMENTAL MEASUREMENT WITH NUMERICAL VALIDATION

Pawel Baranowski, Roman Gieleta, Jerzy Malachowski, Krzysztof Damaziak, Lukasz Mazurkiewicz

Military University of Technology, Faculty of Mechanical Engineering, Department of Mechanics and Applied Computer Science, Gen. S. Kaliskiego 2, 00-908 Warsaw, Poland (✉ pbaranowski@wat.edu.pl, +48 22 683 9683)

Abstract

Materials and their development process are highly dependent on proper experimental testing under wide range of loading within which high-strain rate conditions play a very significant role. For such dynamic loading Split Hopkinson Pressure Bar (SHPB) is widely used for investigating the dynamic behavior of various materials. The presented paper is focused on the SHPB impulse measurement process using experimental and numerical methods. One of the main problems occurring during tests are oscillations recorded by the strain gauges which adversely affect results. Thus, it is desired to obtain the peak shape in the incident bar of SHPB as "smooth" as possible without any distortions. Such impulse characteristics can be achieved using several shaping techniques, e.g. by placing a special shaper between two bars, which in fact was performed by the authors experimentally and subsequently was validated using computational methods.

Keywords: Split Hopkinson Pressure Bar, impulse measurement, experimental testing, numerical studies.

1. Introduction

The Kolsky bar, more commonly known as Hopkinson bar, is widely used to investigate the dynamic behaviour of solid materials at high strain rates within the range of 10^2 to 10^4 s^{-1} [1-11]. The device is named after John Hopkinson and his son Bertram [2, 3, 12, 13]. In 1872 John investigated a stress wave propagation in a wire [2, 12] which resulted in the development of the movement recording method of a cylinder during strongly dynamic conditions [3,13] by his son Bertram. Later in 1948 Davies improved this technique with better accuracy of measured data, e.g. pressure versus time history curves [14]. One year later Kolsky used two elastic bars instead of one with the specimen placed between them [15]. Since then, this device has been known as the Split Hopkinson Pressure Bar (SHPB) or Kolsky bar.

The aforementioned SHPB is used for obtaining stress-strain curves of investigated materials for certain strain rate. However such investigations are exposed to the problems of oscillations recorded by the strain gauges, called Pochhammer-Chree oscillations [14, 16] which adversely affect results. Therefore it is significant to obtain constant strain rate conditions during tests [1, 17, 18], as well as stress equilibrium in a specimen [5, 19, 20]. This can be achieved by adjusting the incident pulse shape, which has a direct influence on material behavior. Several methods can be used for shaping the incident pulse: e.g. by inserting a preloading bar [1, 19, 21], modifying the shape of the striker bar [22, 23-28] or using a pulse shaper [1, 5, 18, 19, 29-33], which was investigated by the authors.

This paper is focused on incident pulse measurement and shaping methodology using experimental tests and numerical methods. The use of a pulse shaper is a simple experimental

procedure, but in order to obtain a constant strain rate during tests many attempts have to be conducted. This can be easily achieved using numerical methods more particularly finite element method, which was presented by other authors [28-33]. Similarly to these papers, the authors of the paper present the numerical modeling of a pulse shaper using typical finite Lagrangian elements and additional meshless Smoothed Particle Hydrodynamics method (SPH). According to the authors knowledge, SPH is particularly well suited to the problems where large deformations of the analysed structure occur. Therefore, it is expected that this method will be very effective in terms of shaper behavior modeling.

It should be stated that such a concept of shaper modeling using a meshless method (more particularly SPH), besides FE modelling, seems to be novel and original. The authors have not came across a similar work that covers the study of different methods of wave shaper modeling with their experimental validation.

Both methods used are available in explicit LS-Dyna code, which was also used by the authors for performing numerical simulations. The presented paper is the part of wider investigations which are aimed at finding the optimal shape of an incident pulse for a specific type of material (brittle, ductile or soft). This can be obtained using the discussed shapers or with a special shape of the striker, which in fact was the investigation object of the previous authors' paper [28].

2. SHPB pressure impulse measurement

Experimental pressure impulse measurement was performed on the conventional SHPB apparatus (Fig 1). Basically, the device consists of a gas gun, a striker (*20 mm* diameter, *150 mm* long), copper pulse shaper (*5 mm* diameter, *3 mm* long), an incident bar, a transmission bar (both *20 mm* diameter and *2000 mm* long), an energy absorption element and a data acquisition system. The striker is launched using highly compressed gas and impacts the incident bar. This generates the elastic wave (incident wave) which travels through the bar and then, due to the difference between mechanical impedances of bar and specimen materials, part of the pulse comes back (reflected wave), whereas the rest of it is transmitted through the tested specimen. Consequently, the wave travels to the transmission bar and generates a so-called transmitted wave (Fig. 2). All three signals are sensed by strain gauges which are placed in the middle of the bars.

For the purpose of pressure bar signal measurements, strain gauges connected in a quarter bridge configuration are used. EA-06-060LZ-120 strain gauges are attached at the longitudinal centres of the incident and transmitted bars. The signal from the strain gauge (from the Wheatstone bridge) is of the order of millivolts, therefore a signal amplifier is necessary to accurately record the low-amplitude voltage. In the SHPB apparatus, a transient amplifier LTT 500 (LTT Labortechnik Tasler GmbH, Germany) and high-speed A/D computer board NI USB-6366 (National Instruments, USA) are used (Fig. 1). In a typical SHPB experiment, the minimum frequency response of all the components in the data-acquisition system should be 100 kHz. In the described apparatus, the amplifier and the A/D computer board have a 1MHz frequency response what allows to accurately record the transient signals from the strain gauges. Also, the bandwidth of the LTT 500 amplifier for strain gauge inputs was 1MHz. In the set-up, the signals are recorded digitally with a *0.5 µs* sampling step, thus the sampling frequency was 2 MHz in each channel.
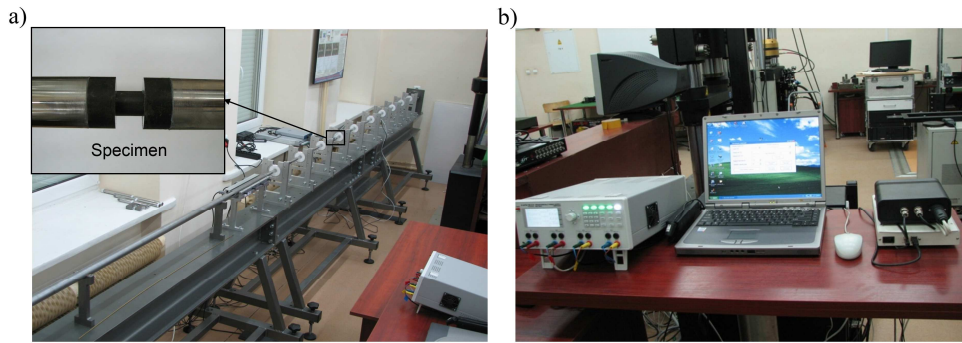
Fig. 1. a) Split Hopkinson Pressure Bar apparatus with data acquisition system and b) control system.

During experimental investigation the pulse in the incident bar was shaped by the copper disk inserted between the striker and incident bar. The plastic deformation of the pulse shaper physically filters out the high frequency components (above 40 kHz) in the incident pulse, as a result wave dispersion was significantly minimized.

Most types of electrical resistance strain gauges are usually adequate for studying wave propagation problems. The size of the gauge is dependent on the highest significant frequency (or shortest wavelength) of the signal. The authors estimated the maximum length from the equation [34]:

$$L = \frac{1}{10f}\sqrt{\frac{E}{\rho}},$$ (1)

where: L is the gauge length, f is the highest significant frequency, and E and ρ are Young's modulus and density of the incident bar material, respectively.

Taking into account the material of the incident bar (maraging steel) and the highest significant frequency in the signal, the estimated maximum length was $L = 10.7\ mm$. In the set-up EA-06-060LZ-120 strain gauges with length $L = 1.52\ mm$ were used, what indicates that the influence of strain-gauge dynamic response on the results can be neglected.

In Fig. 2 the wave propagation is presented. Based on the foregoing it can be concluded that the pulse duration time increases proportionally with increasing striker bar length [1, 2, 9, 10, 12, 15, 20]:

$$T = \frac{2L}{c_p},$$ (2)

where: T is the impulse duration time, L is the striker length and c_p is the elastic wave propagation velocity in the bar material.
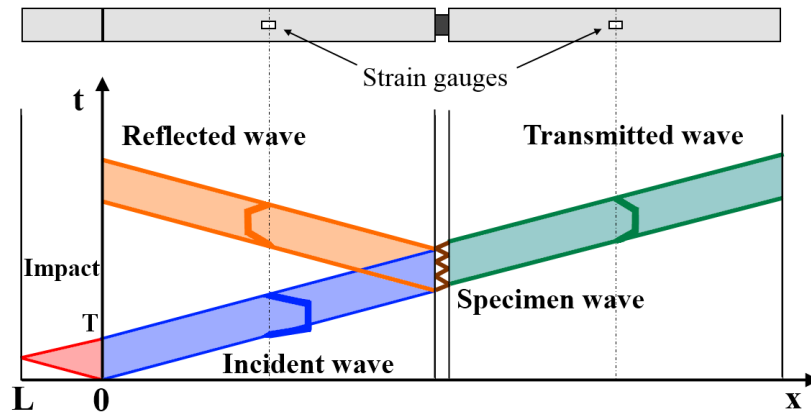
Fig. 2. Wave history route in SHPB.

For the purpose of the paper, experimental measurements of the impulses were carried out. As a result, signals from the strain gauges placed on incident and transmitted bars were obtained (Fig 3).
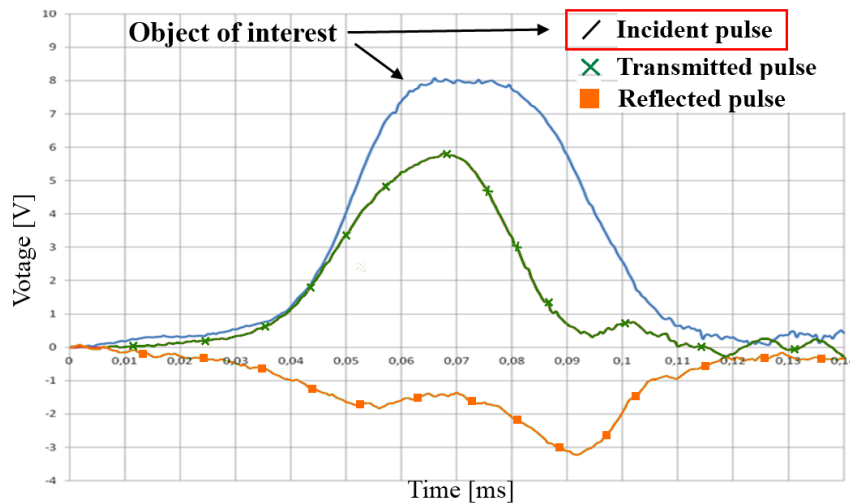

Fig. 3. Three pulses obtained from experimental tests.

In the presented investigations the incident pulse is the main object of interest, which shape has a direct influence on material behavior during tests. In Fig. 3 the incident pulse is "streamlined" and sinusoidally shaped without any oscillations, which was caused by the copper pulse shaper inserted between the striker and the incident bar. It is well documented [1, 5, 17-20] that such impulse shape gives the possibility to obtain constant strain rate conditions during tests, as well as stress equilibrium in the specimen (for the specific family of materials). Now, when the specimen is in a state of uniform stress, the relationship between three pulse proceedings (transmitted, incident and reflected) can be described by [1, 2, 9, 10, 12, 15, 20]:

$$\varepsilon_T(t) = \varepsilon_I(t) - \varepsilon_R(t). \qquad (3)$$

According to the conventional one-dimensional SHPB theory, the nominal strain rate, strain and nominal stress in the specimen are given by [1, 2, 9, 10, 12, 15, 20]:

$$\varepsilon(t) = -2\frac{C_0}{L_S}\varepsilon_R(t), \qquad (4)$$

$$\varepsilon(t) = -2\frac{C_0}{L_S}\int_o^t \varepsilon_R(t)dt, \qquad (5)$$

$$\sigma(t) = -\frac{ES_{p0}}{S_{pr}}\varepsilon_T(t), \qquad (6)$$

where : C_o – is the wave velocity in the incident bar, L_s – is the specimen length, E – Young's modulus, S_{po} – is the cross section area of transmitted bar, S_{pr} – is the cross section area of the specimen, $\varepsilon_R(t)$ – is the reflected strain history, $\varepsilon_T(t)$ – is the transmitted strain history.

3. Numerical modeling

Numerical simulations in the presented study were performed using the aforementioned explicit LS-Dyna solver with a central difference scheme and with the implementation of a modified equation of motion time integration [35]. In the carried out analyses the stability of computations was guaranteed by the Courant-Friedrichs-Lewy (CFL) condition which states that a necessary condition for the convergence of an explicit scheme is that the domain of dependence of the discrete problem includes the domain of dependence of the differential equation in the limit as the length of the finite difference steps goes to zero [35]:

$$C = \frac{u_x\Delta t}{\Delta x} + \frac{u_y\Delta t}{\Delta y} + \frac{u_z\Delta t}{\Delta z} \le C_{max}, \qquad (7)$$

where: u_x, u_y, u_z are the velocities, Δt is the time step, Δx, Δy, Δz are length intervals, C_{max} varies with the method used (in the presented investigations it was set to the default C_{max}=0.9).

With the use of the finite element method a numerical model of the SHPB apparatus was developed and initially validated. The authors were focused only on the incident wave so the specimen, stopper and transmission bars were omitted. Also, in order to simplify and shorten computational time, symmetry of the problem was assumed and only a quarter of the model was taken into consideration. A more detailed description of SHPB apparatus modeling can be found in the previous authors' paper [28].

Initial velocity conditions were applied to the whole striker volume (all nodes), which value exactly corresponded to the actual one, e.g. *v= 29.5 m/s*. Due to the fact that in the presented numerical investigations the impulse is shape strongly depended on a proper contact procedure definition. Thus, it was necessary to simulate the interaction between the segments of collaborating parts as accurately as possible using the penalty function approach [35], which is added to the basic FEM system of equations:

$$\pi(u) = \kappa[(Bu - g_N)^T (Bu - g_N)], \qquad (8)$$

where: u is the global displacement vector, κ is the fictional elastic element stiffness, B is the matrix of boundary conditions kinematics, g_N is the initial vector between the node and the segment in contact.

Material properties for the bars were described with a typical Hooke's law elastic constitutive model (with literature steel data) since the incident and striker bars remain elastic during tests [1]. It is well known that the maximum stresses rise with increasing strain rates, which also influence yielding of the material (Fig. 4). In the presented studies the copper shaper deforms in dynamic conditions where the strain rate plays great importance. Thus, in both cases (FE and SPH modeling) the Johnson-Cook constitutive material model was utilized in the modeling of the copper pulse shaper. It provides a prediction of flow stress σ_{flow}

for large strains and high strain rates, where its dependence on strain rate is linear in a semi- logarithmic scale [35, 36]:

$$\sigma_{flow} = \left[A + B \left(\varepsilon^p \right)^n \right] \left(1 + C \, ln \, \dot{\varepsilon}^p_* \right), \tag{9}$$

where A, B, C, n are material constants, ε^p – is the effective plastic strain, $\dot{\varepsilon}^p_*$ – is the effective plastic strain rate.

In Table 1 constants for J-C material implemented in the investigations are listed [35, 36]:

Table 1. Properties of copper for the J-C constitutive material model used in analyses.

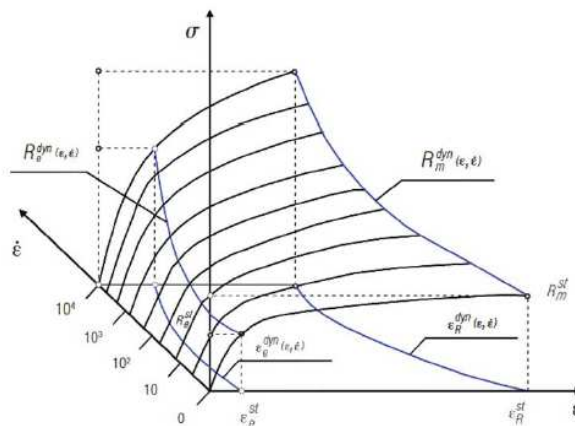| A [MPa]	B [MPa]	N	C	ρ [kg/m3]	E [GPa]	υ
92	292	0.310	0.025	1.09	115	0.33

Fig. 4. Influence of strain rate on the yielding process of steel material [10].

The Grüneisen equation of state was used for describing the pressure-volume relationship of the copper pulse shaper with constants taken from [37] (Table 2). It defines the pressure for compressed materials as [35]:

$$p = \frac{\rho_0 C^2 \mu \left[1 + \left(1 - \frac{\gamma_0}{2} \right) \mu - \frac{a}{2} \mu^2 \right]}{\left[1 - (S_1 - 1)\mu - S_2 \frac{\mu^2}{\mu+1} - S_3 \frac{\mu^3}{(\mu+1)^2} \right]^2} + (\gamma_0 + a\mu)E, \tag{10}$$

and for expanded materials as [35]:

$$p = \rho_0 C^2 \mu + (\gamma_0 + a\mu)E, \tag{11}$$

where C is the intercept of the v_s-v_p curve, S_1, S_2 and S_3 are the coefficients of the slope of the v_s-v_p curve, γ_0 is the Grüneisen gamma, a is the first-order volume correction to γ_0, and $\mu = \frac{\rho}{\rho_0} - 1$.

Table 2. Constants required for input in the Grüneisen EOS.

C_0 [m/s]	S_1	S_2	S_3	γ_0	a
3933	1.5	0	0	1.99	0.5

With the implementation of the finite element method the incident pulse was measured and consequently compared with the experimental data. As stated before, two different cases were taken into consideration:

    – with pulse shaper modeled using typical Lagrangian elements,
    – with pulse shaper modeled using the meshless SPH method.

3.1. FE copper shaper modeling

The FE model of the copper pulse shaper consisted of 1036 elements and 1445 nodes (Fig. 5). The shape of elements was selected to be extended, which provided better accuracy and stability of computations throughout the analysis in which the copper sample becomes largely compressed. The interaction between the striker, bars and shaper was described by the surface-to-surface contact procedure and no friction was assumed, which in actual conditions is practically zero and is provided by lubricating contact surfaces.

3.2. SPH copper shaper modeling

The SPH model of the shaper (with the same dimensions as previously) consisted of 468 elements with the average distance between particles 0.035 mm (Fig. 5). In this case the interaction between the SPH shaper, Lagrangian striker and the bar was described by the nodes-to-surface contact procedure. Identically to the previous case no friction was assumed. Also, it was found that when SPH particles are used in simulation, default values for the artificial bulk viscosity for Lagrange solid elements are not appropriate [38]. Thus, in the presented investigations the authors used recommended values for SPH formulation: $Q_1 = 1.5$ and $Q_2 = 1.0$. The described parameter is significant in SPH due to the prevention of interparticle penetration and allows shocks to form and to damp post-shock oscillations.
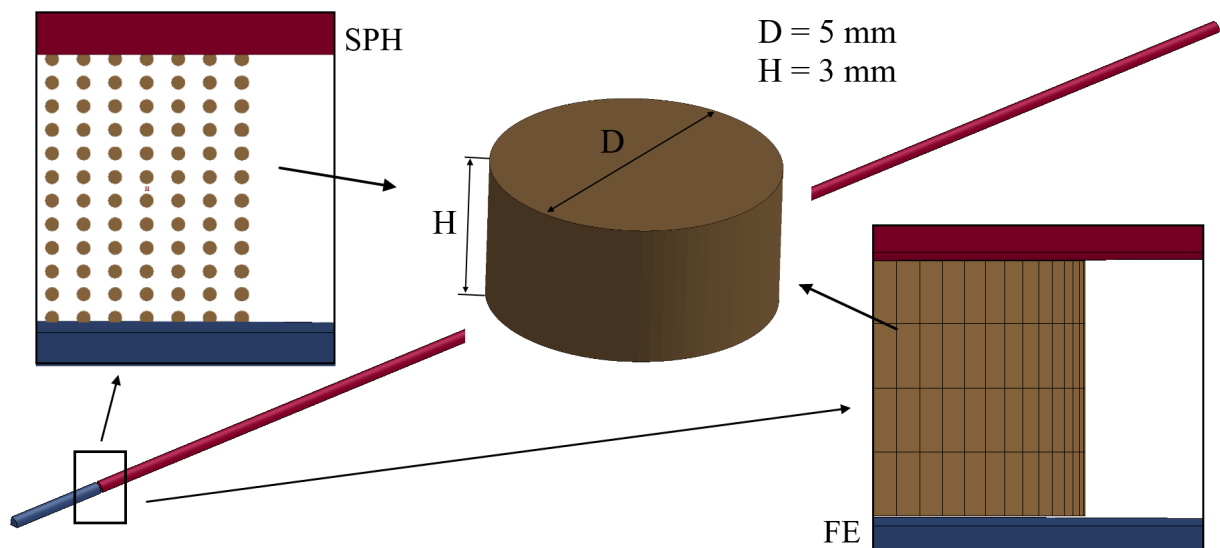

Fig. 5. FE and SPH pulse shaper between striker and incident bar.

Smoothed Particles Hydrodynamics is a mesh-free particle method with Lagrangian nature, where computational information including mass and velocity is carried with particles. This method is mainly used for simulating fluid flows and large deformations of structures. The main difference between classical methods and SPH is the absence of a grid. Therefore, those particles are the framework of the region within which the governing equations

are solved [35]. The SPH method uses the concept of kernel and particle approximation as follows [35]:

$$\prod^{k} f(x) = \int f(y)W(x-y,h)dy \,,$$ (12)

where W denotes a function which is defined using the function θ by the relation:

$$W(x,h) = \frac{1}{h(x)^{d}}\theta(x) \,,$$ (13)

where d is the number of space dimensions and h is the so-called smoothing length which varies in time and in space.
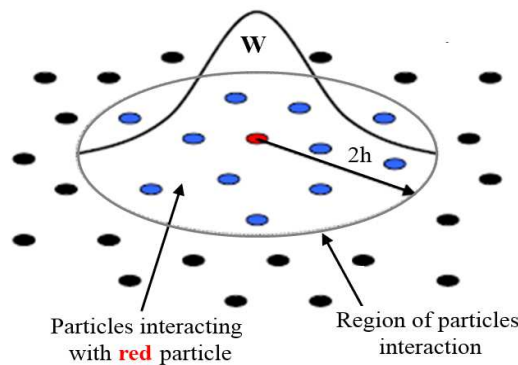

Fig. 6. SPH method schematic presentation [39].

4. Impulse measurement results and discussion

As stated before, the main aspect of the investigated issue was to measure and compare incident impulses obtained from experimental and numerical tests. Firstly, however the deformation of the copper shapers (actual and virtual) will be presented and compared. In Fig. 7 deformation of the model in both cases is shown for three different moments of time during simulation. Great similarity in the behavior of both samples can be noticed, which proves that the implemented parameters, material characteristics and boundary conditions were used appropriately. Moreover, by comparing diameter and length after the impact we can also see good correlation between results (Table 3).
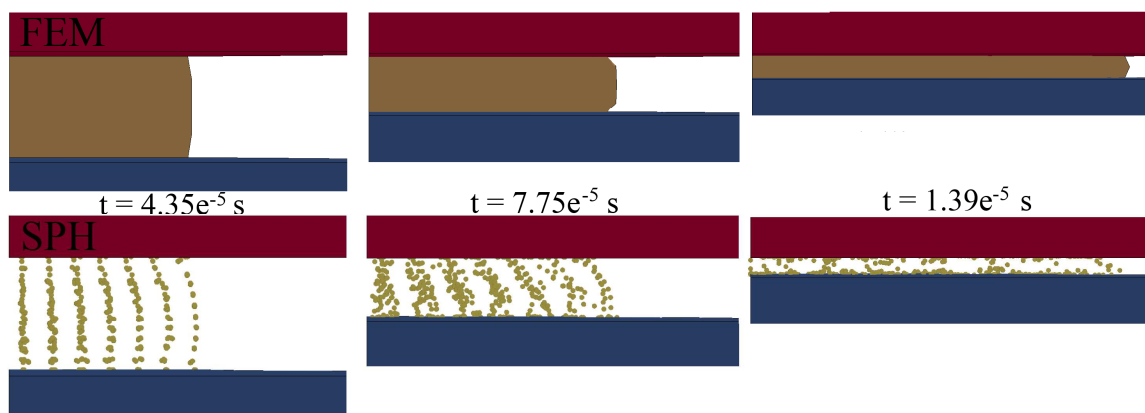

Fig. 7. Copper shaper deformation comparison for both cases.

Table 3. Shaper dimensions after impact comparison.

	Experimental	FEM	SPH
Diameter [mm]	~14.6	~13.6	~14.2
Length [mm]	~0.35	~0.41	~0.37

Finally, measured incident impulse characteristics (stress) were examined and compared (Fig. 8). In the simulations pulse characteristics were taken from the incident bar element which directly corresponded to the place where the strain gauge was glued.

As expected from the previous results showing deformation and diameter comparison, quite good agreement can be seen for all three measurements. This leads us to the conclusion that despite of different methods used in computations, all result in similar behavior of the shaper during the simulations. Also, all three impulses have nearly the same duration time which, from the physical point of view, is correct and also shows that the formula in Equation (1) is satisfied.

However, better correlation between experimental and numerical impulses could be obtained with proper material parameters estimated during dynamic compression testing on the SHPB. Nevertheless, the main intention of the authors was to present a possibility of numerical methods implementation in SHPB testing, more particular, in investigating wave effects.
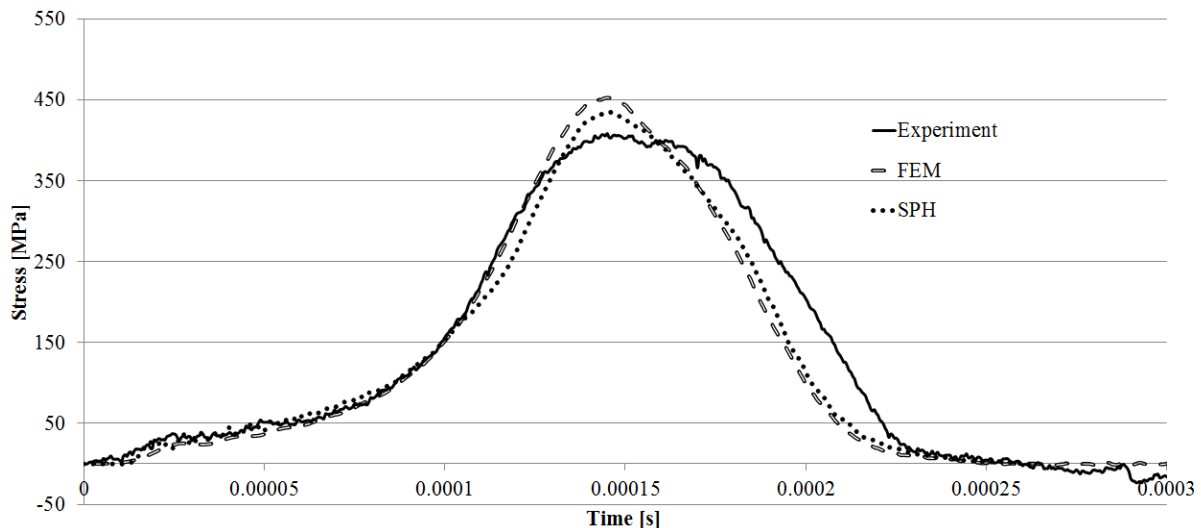

Fig. 8. Impulse shape comparison (experimental and numerical).

5. Conclusions

In the presented paper the authors have undertaken modeling the SHPB apparatus during its operation with particular attention pointed at wave effects (impulses) investigation. Numerical simulations were performed with two different methods of copper shaper modeling chosen from the LS-Dyna software: typical finite element formulation (Lagrange) and a more sophisticated Smoothed Particles Hydrodynamics (SPH) method. As a result, overall deformation of the shaper was obtained and compared with each other. However, the main emphasis was placed on the impulse measurement and its testing. Results show that numerical modeling can be very useful in SHPB with pulse shaper investigations. In experimental procedure many attempts have to be conducted for finding proper shaper dimension that will guarantee constant strain rate during tests. This can be easily achieved using numerical

methods. Moreover, with proper constitutive material modeling computation methods give the possibility to initially verify experimental set-up parameters, before the final testing.

It seems that SPH modeling gives underestimated stress values and this needs to be verified in subsequent analyses with experimental validation. Also for such short-lasting simulations of SHPB, the time needed to prepare the model with SPH is disproportionate (the method is vulnerable to the regularity of particle distribution and parameters used). However, when the method is understood with all its options learned, it can be very effective. In FE modelling of the copper shaper special care must be taken to choose a proper aspect ratio of elements. In addition to being largely compressed they also maintain contact with the bars so the accuracy of contact definition as well as stability of computations needs to be satisfied.

Thus, both methods in terms of SHPB numerical testing have some disadvantages, but all in all, FE modeling seems to be more suitable for such phenomena.

Nevertheless, the obtained and tested numerical methods will be more thoroughly studied in the next stages of investigations and will be extended by adding another, more sophisticated, method of pulse shaper modeling. Also, in subsequent stages copper and other materials used for shapers will be experimentally tested for obtaining the constitutive material parameters. The presented paper is part of the study aimed at finding an ideal shape of the incident pulse for a specific type of material as brittle, ductile or soft which will give the possibility to perform experimental tests in constant strain rate conditions and with stress equilibrium in a specimen.

Acknowledgements

References

[1] Ellwood, S., Griffiths, L.J., Parry, D.J. (1982). Materials testing at high constant strain rates. *Journal of Physics E: Scientific Instruments,* 15, 280−282.

[2] Hopkinson, J. (1872). On the rupture of iron wire by a blow. *Proc. Literary and Philosophical Society of Manchester*, 40−45.

[3] Hopkinson, B. (1905). The effect of momentary stress in metals. *Proc. of the Royal Society of London,* 498−507 (1905).

[4] Roland, C.M. (2006). Mechanical behaviour of rubber at high strain rates. *Rubber Chemistry and Technology*, 79, 429–459.

[5] Song, B., Chen, W. (2005). Split Hopkinson pressure bar techniques for characterizing soft materials. *Latin American Journal of Solid and Structures*, 2, 113−152.

[6] Chen, W., Lu, F., Frew, D.J., Forrestal, M.J. (2002). Dynamic compressive testing of soft materials. *Journal of Applied Mechanics*, 69, 214−223.

[7] Tasneem, N. (2005). *Study of wave shaping techniques of split hopkinson pressure bar using finite element analysis*, Ph.D. Thesis. Graduate School of Wichita State University.

[8] *Hopkinson pressure bar using finite element analysis*, Ph.D. Thesis. Graduate School of Wichita State University.

[9] Parry, D.J., Walker, A.G., Dixon, P.R. (1995). Hopkinson bar pulse smoothing. *Measurement Science and Technology*, 6, 443−446.

[10] Janiszewski, J. (2012), *The study of engineering materials under dynamic loading*, Military University of Technology, Warsaw.

[11] Chmielewski, R., Kruszka L., Młodożeniec, W. (2004), The study of static and dynamic properties of 18G2 steel, *Biuletyn WAT*, 53, 31–45.

[12] Nowacki, W. K., Klepaczko, J. R. (2001). *New Experimental Methods in Material Dynamics and Impact*. Centre of Excellence for Advanced Materials and Structures, Polish Academy of Sciences, Warsaw.

[13] Hopkinson, J. (1872). Further experiments on the rupture of iron wire. *Proc. Literary and Philosophical Society of Manchester*, 119–121.

[14] Hopkinson, B. (1914). A method of measuring the pressure produced in the detonation of high explosives or by the impact of bullets. *Philosophical Transactions of the Royal Society of London*, 213, 437–456.

[15] Davies, R.M. (1948). A critical study of the Hopkinson pressure bar. *Philosophical Transactions of the Royal Society of London*, 240, 375–457.

[16] Kolsky, H. (1949). An investigation of the mechanical properties of materials at very high rates of loading. *Proc. of the Physical Society*, 62, 676–700.

[17] Graff, K.F. (2004). *Wave Motion in Elastic Solids*. Dover Publications. New York.

[18] Song, B., Chen, W. (2004). Dynamic stress equilibration in split Hopkinson pressure bar tests on soft materials. *Experimental mechanics*, 44(3), 300–312.

[19] Frew, D.J., Forrestal, M.J., Chen, W. (2002). Pulse shaping techniques for testing brittle materials with a split Hopkinson pressure bar. *Experimental mechanics*, 42 (1), 93–106.

[20] Foley, J.R., Dodson, J.C., McKinion, C.M. (2010). Split Hopkinson Bar Experiments of Preloaded Interfaces. *Proc. of the IMPLAST 2010 Conference*.

[21] Vecchio, K.S., Jiang, F. (2007). Improved Pulse Shaping to Achieve Constant Strain Rate and Stress Equilibrium in Split-Hopkinson Pressure Bar Testing. *Metallurgical and materials transactions A*, 38, 2655–2665.

[22] Franz, C.E., Follansbee, P.S., Berman, I., Schroeder, J.W. (1984). *High energy rate fabrication*. American Society of Mechanical Engineers.

[23] Cloete, T.J., V.d. Westhuizen, A., Kok, S., Nurick, G.N. (2009). A tapered striker pulse shaping technique for uniform strain rate dynamic compression of bovine bone. *EDP Sciences*, 901–907.

[24] Ramirez, H., Rubio-Gonzalez, C. (2006). Finite-element simulation of wave propagation and dispersion in Hopkinson bar test. *Materials and design*, 27, 36–44.

[25] Ping Yu, Z., De Shun, L., You Duo, P., An Hua, C. (2001). Inverse approach to determine piston profile from impact tress waveform on given non-uniform rod, *Transactions of Nonferrous Metals Society of China*, 11(2), 297–300.

[26] Li, X.B., Lok, T.S., Zhao, J. (2005). Dynamic Characteristics of Granite Subjected to Intermediate Loading Rate. *Rock Mechanics and Rock Engineering*, 38 (1), 21–39.

[27] Seng, L.K. (2003). Design of a New Impact Striker Bar for Material Tests in a Split Hopkinson Pressure Bar. *Civil engineering Research Bulletin*, 16, 70–71.

[28] Wang, L., Xu, M., Zhu, J., Shi, S. (2006). A Method of Combined SHPB Technique and BP Neural Network to Study Impact Response of Materials. *Strain*, 42, 149–158.

[29] Baranowski, P., Malachowski, J., Gieleta, R., Damaziak, K., Mazurkiewicz, L., Kolodziejczyk, D. (2013). Numerical study for determination of pulse shaping design variables in SHPB apparatus, *Bulletin of the Polish Academy of Sciences: Technical Sciences*, 61 (2), 459–466.

[30] Lewis, C.F. (1979). *Properties and selection: nonferrous alloys and pure metals*. Metals Handbook, American Society for Metals.

[31] Baron, H.G. (1956). Stress/strain curves for some metals and alloys at low temperatures and high rates of strain. *The Journal of the Iron and Steel Institute*, 182, 354–365.

[32] Frew, D.J. (2001). *Dynamic Response of Brittle Materials from Penetration and Split Hopkinson Pressure Bar Experiments*. US Army Corps of Engineers, Engineer Research and Development Centre.

[33] Naghdabadia, R., Ashrafia, M.J., Arghavani, J. (2012). Experimental and numerical investigation of pulse-shaped split Hopkinson pressure bar test. *Materials Science and Engineering A*, 539, 285–293.

[34] Benassi, F., Alves, M. (2006). Pulse shaping in the split Hopkinson pressure bar test. *Proc. from the IV National Congress of Mechanical Engineering.*

[35] Doyle, J. F. (1997). *Wave Propagation in Structures. Spectral Analysis Using Fast Discrete Fourier Transforms*, Mechanical Engineering Series, Second edition, Springer.

[36] Hallquist, J.O. (2003). *LS-Dyna:Theoretical manual*. California Livermore Software Technology Corporation.

[37] Johnson, G.R., Cook, W.H. (1983). A constitutive model and data for metals subjected to large strains, high strain rated and high temperatures. *Proc. from the 7th International Symposium on Ballistics*.

[38] Steinberg, D. (1906). *Equation of State and Strength Properties of Selected Materials*. Lawrence Livermore National Laboratory, Livermore, CA.

[39] Schwer, L.E. (2009). Aluminium plate perforation: a comparative case study using Lagrange with erosion, multi-material ALE and Smooth Particle Hydrodynamics. *Proc. from the 7th European LS-DYNA Conference*.

[40] Clearly, P., Das, R. (2008). Modelling Stress Wave Propagation under Biaxial Loading using Smoothed Particle Hydrodynamics. *Proc. from the XXII International Congress of Theoretical and Applied Mechanics*.